Exploring the electrical potential inside cylinders beyond the Debye-Hückel approximation: a computer code to solve the Poisson-Boltzmann equation for multivalent electrolytes

Philippe Leroy, Alexis Maineult

Exploring the electrical potential inside cylinders beyond the Debye-Hückel approximation: a computer code to solve the Poisson-Boltzmann equation for multivalent electrolytes

Philippe Leroy[1] and Alexis Maineult[2*]

[1] BRGM, French Geological Survey, 45060 Orléans, France.

[2] Sorbonne Université, CNRS, EPHE, UMR 7619 METIS, 75005 Paris, France.

[*]Corresponding author:

Tel: +33 (0)1 44 27 43 36

E-mail: alexis.maineult@upmc.fr

Intended for publication in Geophysical Journal International

SUMMARY

The electrical potential at the interface between mineral and water is traditionally computed from the Poisson-Boltzmann (P-B) equation. Nevertheless, this partial differential equation is non-linear and has no analytical solution for cylindrical geometries for instance. For that reason, the linearized P-B equation is mostly used in the literature. In our study, we present a short and easy-to-handle Matlab® code to solve the full (i.e., non-linearized) P-B equation inside a cylinder. Electrical potentials inside amorphous silica and montmorillonite nanotubes, containing NaCl or $CaCl_2$ electrolytes, are computed. The zeta potential, which is an input parameter of our code, is first predicted from basic Stern and extended Stern models. We show that the linearized P-B equation overestimates the electrical potential from the full P-B equation when the zeta potential magnitude is above kT/e ~ 25.7 mV at a temperature T of 298 K with k the Boltzmann's constant and e the electron charge, especially for Ca^{2+} ion in solution. This effect increases when salinity decreases from 0.1 to 0.001 mol L^{-1} because of zeta potentials of higher magnitude, and when the cylinder radius decreases to the nanometric range because of overlapping diffuse layers. Our results may have strong implications for simulating the electrical properties of highly charged nanomaterials such as clays and low-pH cements.

Keywords: Electrical Properties, hydrogeophysics, non-linear differential equations, numerical modelling.

1 INTRODUCTION

Many research areas in Earth sciences, physics, chemistry, and medicine are focused on investigating the electrochemical properties of cylinders (Bocquet & Charlaix 2010; Daiguji 2010; Schoch *et al.* 2008). For instance, in hydrology, the electrical potential on the internal wall of cylinder can be considered in pore network models simulating water flow and solute transport (Li *et al.* 2014; Obliger *et al.* 2014; Xiong *et al.* 2016). It is also used in rock physics to simulate the electrical properties of porous media to interpret, for instance, their self-potential and induced polarization (IP) response (Bernabé 1998; Jougnot *et al.*, 2012; Bücker & Hördt, 2013a). In hydrogeophysics, researchers are actually interested in relating the permeability to the IP response of rocks and, to date, there is a debate about whether it is the grain or pore size that controls it (Revil & Florsch 2010; Revil *et al.* 2012, 2015; Kruschwitz *et al.* 2016; Weller *et al.* 2016). Knowing the electrochemical properties of cylinders is essential to model the induced polarization of rocks using the membrane polarization model and to better assess the effect of pore size on IP (Bücker & Hördt 2013a,b; Bairlein *et al.* 2016; Hördt *et al.* 2016, 2017; Chuprinko & Titov 2017).

In electrokinetics and more generally in hydrogeophysics, most transport models use the zeta potential and the linearized Poisson-Boltzmann equation, based on the Debye-Hückel (D-H) approximation, to model the electrochemical properties of pores (Bernabé 1998; Pride 1994; Conlisk 2005; Schoch *et al.* 2008; Jougnot *et al.* 2012; Bücker & Hördt 2013a). The D-H approximation is accurate for surface electrical potentials, considered equal to zeta potentials, of magnitude inferior or equal to 25.7 mV at a temperature of 25°C (Hunter 1981; Lyklema 1995). Because zeta potentials on mineral surfaces are often much larger, it would be better to use the Poisson-Boltzmann equation without any approximation regarding the surface electrical potential to

compute the electrical potential at the interface between mineral and water (Leroy & Revil 2004; Sverjensky 2005; Vinogradov *et al.* 2010; Li *et al.* 2016). For instance, amorphous silica and the basal surface of montmorillonite, two minerals that are common in the subsurface, exhibit negative zeta potentials that can easily exceed 25.7 mV in magnitude (Rasmusson *et al.* 1997; Sonnefeld *et al.* 2001; Leroy *et al.* 2013, 2015).

As far as we know, there is no code available in the literature to solve numerically the Poisson-Boltzmann equation inside cylinders. We propose a short and easy-to-handle Matlab® code to model the electrochemical properties of cylinders. After a brief presentation of the P-B equation and associated boundary conditions, electrical potential profiles inside amorphous silica and montmorillonite nanotubes, computed from the full and linearized P-B equation, are showed, compared and discussed. Two different electrolytes representative of natural waters, NaCl and $CaCl_2$, are considered, and zeta potentials were computed from well-established surface complexation models describing Stern and diffuse layers at the interface between mineral and water (Leroy *et al.* 2013, 2015).

2. THE POISSON-BOLTZMANN EQUATION INSIDE A CYLINDER

Let us consider a cylinder saturated with an aqueous electrolyte and having its internal wall electrically charged. The distribution of the electrical potential φ (V) in the direction normal to the charged surface is usually computed using the Poisson-Boltzmann (P-B) equation (Hunter 1981; Lyklema 1995; Leroy *et al.* 2010, 2012). The input parameters of this equation are the chemical composition of the bulk electrolyte and the surface electrical potential, often equated with the zeta potential (ζ), or the surface charge density (Hunter 1981; Bourg *et al.* 2007; Leroy *et al.* 2015). The zeta

potential is the surface electrical potential at the plane of shear or slip plane and can be inferred from electrokinetic experiments for instance (Lyklema 1995; Leroy & Revil 2004; Delgado *et al.* 2007; Heuser *et al.* 2012).

The P-B equation can be written as (Appendix A):

$$\nabla^2\varphi = -\frac{1000\,\mathrm{N_A}}{\varepsilon}\sum_{i=1}^{M} q_i C_i \exp\left(-\frac{q_i\varphi}{kT}\right), \tag{1}$$

where $\mathrm{N_A}$ is Avogadro's number (~ 6.022×10^{23} mol^{-1}), ε is the dielectric permittivity of the electrolyte (F m^{-1}), and M is the number of ionic species. The quantity q_i is the ion charge (C), $q_i = es_i$ where e is the elementary charge (~1.602×10^{-19} C) and s_i is the signed ion valence ($s_i = \pm z_i$ with z_i the ion valence, "+" standing for cations and "–" for anions). The quantity C_i is the concentration of ion i (mol L^{-1}, M), k is Boltzmann's constant (~ 1.381×10^{-23} J K^{-1}) and T is the temperature (K). Note that the factor 1000 converts C_i, expressed in mol L^{-1}, into mol m^{-3}.

Eq. (1) can be linearized using the first two terms of the power series of exp(–x) = 1 – x where $x = q_i\varphi / kT$, which works well in the case of small electrical potentials satisfying the condition $|\varphi| << kT / |q_i|$. This yields:

$$\nabla^2\varphi = -\frac{1000\,\mathrm{N_A}}{\varepsilon}\sum_{i=1}^{M} q_i C_i \left(1-\frac{q_i\varphi}{kT}\right). \tag{2}$$

Considering the electroneutrality condition in the bulk electrolyte, i.e.:

$$\sum_{i=1}^{M} q_i C_i = 0, \tag{3}$$

Eq. (2) becomes the Poisson-Boltzmann equation with the Debye-Hückel (D-H) approximation:

$$\nabla^2\varphi = \kappa^2\varphi, \tag{4}$$

where $\chi = \kappa^{-1}$ is the Debye length (m), which is given by:

$$\chi = \sqrt{\frac{\varepsilon kT}{1000\,\mathrm{N_A}\sum_{i=1}^{M} q_i^{\,2} C_i}}\,. \tag{5}$$

Here we consider an infinite cylinder of radius r_0 filled with saline water, with an electrical potential set to ζ on its internal wall. In radial coordinates, Eq. (1) writes:

$$\frac{d^2\varphi(r)}{dr^2} + \frac{1}{r}\frac{d\varphi(r)}{dr} = -\frac{1000\,\mathrm{N_A}}{\varepsilon}\sum_{i=1}^{M} q_i C_i \exp\left[-\frac{q_i\varphi(r)}{kT}\right]. \tag{6}$$

The boundary conditions are:

$$\varphi(r_0) = \zeta\,, \tag{7}$$

and for symmetry reasons:

$$\left.\frac{d\varphi}{dr}\right|_{r=0} = 0\,. \tag{8}$$

Solving Eqs. (6) to (8) allows us to obtain the electrical potential profile $\varphi(r)$. For numerical reasons, it is more convenient to solve a dimensionless equation. For that purpose, we replaced in Eq. (6) the quantity q_i by es_i – by doing so, the electronic charge is taken out of the summation. Eq. (6) thus becomes:

$$\frac{d^2\varphi(r)}{dr^2} + \frac{1}{r}\frac{d\varphi(r)}{dr} = -\frac{1000\,\mathrm{N_A}\,e}{\varepsilon}\sum_{i=1}^{M} s_i C_i \exp\left[-\frac{s_i e\varphi(r)}{kT}\right]. \tag{9}$$

We define the following quantities:

$$R = \frac{r}{\chi}\,, \tag{10}$$

which is the dimensionless radius;

$$\Phi(R) = \frac{e\varphi(r)}{kT}\,, \tag{11}$$

which is the dimensionless electrical potential; and

$$\xi = \frac{e\zeta}{kT}\,, \tag{12}$$

which is the dimensionless zeta potential.

Eq. (9), (7) and (8) then become:

$$\frac{d^2\Phi}{dR^2}+\frac{1}{R}\frac{d\Phi}{dR}=-\frac{\sum_{i=1}^{M} s_i C_i \exp\left(-s_i\Phi\right)}{\sum_{i=1}^{M} s_i^2 C_i}, \tag{13}$$

$$\Phi\left(R_0\right)=\xi, \tag{14}$$

$$\left.\frac{d\Phi}{dR}\right|_{R=0}=0\,. \tag{15}$$

Eqs. (13) to (15) were rewritten in a form usable by the Matlab® procedure bvp4c, which solves ordinary differential equations given their boundary conditions using the collocation method. The code, which computes $\Phi(R)$ and then $\varphi\left(r\right)$, is presented in Appendix B.

Finally, let us consider the Poisson-Boltzmann equation in radial coordinates with the Debye-Hückel approximation (from Eq. (4)):

$$\frac{d^2\varphi\left(r\right)}{dr^2}+\frac{1}{r}\frac{d\varphi\left(r\right)}{dr}=\frac{1}{\chi^2}\varphi\left(r\right). \tag{16}$$

The solution for the boundary conditions (7) and (8) is given by (e.g., Bernabé 1998):

$$\varphi\left(r\right)=\zeta\frac{\mathrm{J}_0(i\,{}^{r}\!/_{\chi})}{\mathrm{J}_0(i\,{}^{r_0}\!/_{\chi})}, \tag{17}$$

where J_0 is the zero-order modified Bessel function of the first kind and *i* the imaginary number.

3. APPLICATIONS TO AMORPHOUS SILICA AND MONTMORILLONITE NANOTUBES

We used our code to compute the electrical potential profiles inside cylinders

assuming amorphous silica or montmorillonite surfaces. These two minerals are of particular interest because silicon dioxide is often used in nanofluidics (Schoch *et al.* 2008; Bocquet & Charlaix 2010; Daiguji 2010). It is also the major compound of quartz sand and sandstones, which are very common in the subsurface (Leroy *et al.* 2008; Vinogradov *et al.* 2010; Revil *et al.* 2015), and one of the main constituents of cement (Labbez *et al.* 2006; Grangeon *et al.* 2013; Lerouge *et al.* 2017). Montmorillonite is often found in sedimentary soils and rocks, and is the major compound of bentonite, which is used for instance for the ground storage of domestic wastes and underground storage of highly radioactive and long-lived nuclear wastes (Malusis *et al.* 2003; Rotenberg *et al.* 2007; Tournassat *et al.* 2013; Leroy *et al.* 2015, 2017).

We consider cylindrical pores of diameters 10, 100, and 1000 nm, and containing 1:1, NaCl, or 2:1, $CaCl_2$, salts of concentrations 1, 10 and 100 mM at a temperature of 25°C (mM stands for 10^{-3} mol L^{-1}). Pore diameters and chemical compositions of the bulk electrolyte were chosen to encompass values typical for nanopores containing monovalent and multivalent electrolytes (Dufreche *et al.* 2001, 2005; Wang & Revil 2010; Wang *et al.* 2010). These salts were also chosen because they contain some major ions found in natural waters (McCleskey 2011). Electrochemical properties of amorphous silica were investigated as a function of pH because of the presence of silanol surface sites exchanging protons with surrounding electrolyte, responsible for its negative surface charge and zeta potential (Sonnefeld *et al.* 2001). Those of the basal surface of montmorillonite were considered independent on pH because of its permanent negative surface charge and zeta potential due to ion substitution in the crystal (Tournassat *et al.* 2011).

3.1 Surface complexation models

Zeta potentials were computed using the surface complexation models of Leroy *et al.* (2013) for amorphous silica and Leroy *et al.* (2015) for the basal surface of montmorillonite, considering the additional adsorption of calcium ions in the Stern layer. They were not measured because of the high uncertainties associated with interpretation of electrokinetic measurements into zeta potentials (Hunter 1981; Lyklema 1995; Delgado *et al.* 2007). In the surface complexation models of Leroy *et al.*, the charged surface does not electrostatically interact with another charged surface. Therefore, one limitation of our approach is that the zeta potentials are computed using one plane surface in contact with an infinite electrolyte where electroneutrality occurs in the bulk part. To properly consider interacting diffuse layers when the pore is completely filled by them, it would be better to develop a P-B code considering as input parameter the surface charge density rather than the zeta potential. Nevertheless, actual geophysical codes are more familiar with the zeta potential than the surface charge density (Vinogradov *et al.* 2010; Jougnot *et al.* 2012; Bücker & Hördt 2013a). Therefore, developing a P-B code considering as input surface charge density rather than zeta potential will be carried out in the future when geophysical codes will also consider this input parameter.

Electrostatic surface complexation models describe electrical potential and ion distributions at the mineral/water interface (Gouy 1910; Chapman 1913). Their input parameters typically are the temperature, chemical composition of the bulk electrolyte, total density of surface groups, equilibrium adsorption constants of the protons and counter-ions, and capacitance(s) (Hiemstra *et al.* 1989). In the triple layer model (TLM) or extended Stern model (Fig. 1), the "0-plane" corresponds to the surface of the mineral where protonation and deprotonation reactions occur, the "β-plane" is located at the center of the compact Stern layer made of adsorbed counter-ions, and the "*d*-plane"

delimits the onset of the diffuse layer containing counter-ions and co-ions (Yates *et al.* 1974). The basic Stern model (BSM) is a simplified TLM where the "*β*-plane" coincides with the "*d*-plane" (no capacitance necessary to describe the electrical potential between these two planes, Westall & Hohl 1980). In these two models, the zeta potential, *ζ*, which is the electrical potential at the shear plane, is traditionally assumed to be located slightly further way from or at the "*d*-plane" because no water flow is considered between the mineral surface and the onset of the diffuse layer (Hunter 1981; Lyklema *et al.* 1998).

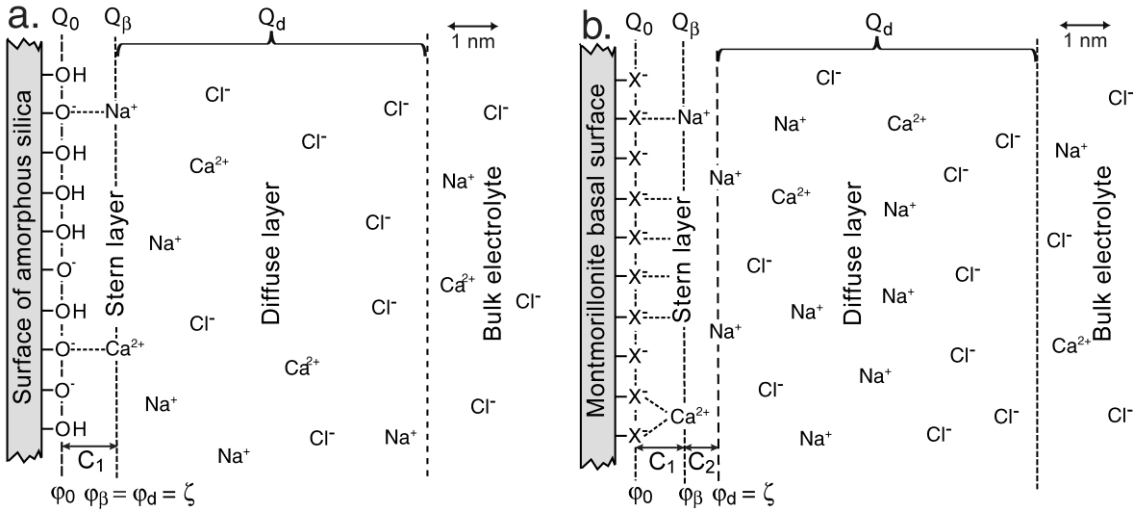

Figure 1. Sketch of the surface complexation models to compute the zeta potential (ζ) for amorphous silica (BSM, a., modified from Leroy *et al.* 2013) and montmorillonite (TLM, b., modified from Leroy *et al.* 2015). The symbols φ, Q, and C respectively represent the electrical potential, surface charge density, and capacitance. Note the different types of surface sites, with the silanols >Si-OH for amorphous silica and $>X^-$ resulting from isomorphic substitutions in the solid for montmorillonite.

Besides zeta potential measurements, and tritium experiments and crystallographic considerations for the total surface site densities, one way to calibrate the parameters of the surface complexation model (the adsorption equilibrium constants and capacitance(s)) is to use surface charge density measurements from acid-base potentiometric titration and cation exchange capacity (CEC) (Tournassat *et al.* 2004; Bourg *et al.* 2007; Leroy *et al.* 2013, 2015).

3.1.1 Amorphous silica

The negative surface charge density of amorphous silica arises from the deprotonation of the silanol surface sites >SiOH to form >SiO$^-$ surface species. It attracts cations in the Stern layer. Surface charge density measurements of amorphous silica nanoparticles, Degussa Aerosil 380 of average size 7 nm, in contact with NaCl or $CaCl_2$ electrolytes (Dove & Craven 2005), were used to adjust the adsorption equilibrium constants of the Na^+ and Ca^{2+} counter-ions in the Stern layer (Table 1). For that purpose, the following cost function, based on the least-square method (Caceci & Cacheris 1984), was minimized for each electrolyte using the gradient method:

$$R = \sqrt{\sum_{i=1}^{P} w_i \left[Q_{0cal}(i) - Q_{0obs}(i) \right]^2}\,, \tag{18}$$

where P is the number of surface charge density measurements for each electrolyte, w_i is a weighting coefficient (we took $w_i = 1$), and Q_{0cal} and Q_{0obs} are the calculated and measured surface charge density, respectively (C m^{-2}). The other parameters of the BSM, which are the total surface site density Γ_S, the equilibrium adsorption constant of the H^+ ion and the C_1 capacitance, were set following the work of Hiemstra *et al.* (1989): $\Gamma_S = 4.6$ sites nm^{-2}, $\log K_{\mathrm{Si,H}} = 7.5$ and $C_1 = 3.3$ F m^{-2} (Table 2). The detailed procedure to compute the surface charge density is explained in Leroy *et al.* (2013). It was calculated as a function of the computed surface sites densities Γ_i using (Davis *et al.* 1978; Leroy & Revil 2004):

$$Q_{0cal} = -e\left(\Gamma_{>\mathrm{SiO}^-} + \Gamma_{>\mathrm{SiO}^- - \mathrm{M}^+}\right), \tag{19}$$

where $\Gamma_{>\mathrm{SiO}^-}$ and $\Gamma_{>\mathrm{SiO}^- - \mathrm{M}^+}$ are respectively the surface site densities of deprotonated silanols and adsorbed counter-ions in the Stern layer (sites m^{-2}), which were computed with Matlab using the approach of Leroy *et al.* (2013).

Table 1. Ion adsorption reactions on amorphous silica.

Surface complexation reactions	"0-plane"	"β-plane"	Adsorption constants
$>SiO^- + H^+ \Leftrightarrow >SiOH$	+1	0	$K_{Si,H}$
$>SiO^- + Na^+ \Leftrightarrow >SiO^- - Na^+$	0	+1	$K_{Si,Na}$
$>SiO^- + Ca^{2+} \Leftrightarrow >SiO^- - Ca^{2+}$	0	+2	$K_{Si,Ca}$

Table 2. Parameters of the basic Stern model for amorphous silica.

Parameters	Values
Log(H^+ adsorption constant) Log$K_{Si,H}$	7.5 [1]
Log(Na^+ adsorption constant) Log$K_{Si,Na}$	–3 [2]
Log(Ca^{2+} adsorption constant) Log$K_{Si,Ca}$	–0.5 [2]
Total surface site density Γ_S (nm^{-2})	4.6 [1]
Inner capacitance C_1 ($F\ m^{-2}$)	3.3 [1]

[1] From Hiemstra *et al.* (1989).
[2] Optimized according to the surface charge density measurements of Dove & Craven (2005).

Predicted surface charge densities of amorphous silica nanoparticles are showed in Fig. 2a. Our surface complexation model reproduces very well increasing magnitude of the negative surface charge density when pH and salinity increases, observed especially in the case of $CaCl_2$ electrolyte because of the adsorption constant of Ca^{2+} ions higher than for Na^+ ions in the Stern layer (Table 2). Negative zeta potentials predicted for the chemical conditions of electrical potential calculations inside cylinders are presented in Fig. 2b. Calculated zeta potential increases in magnitude when pH increases and salinity decreases, especially for NaCl electrolyte because of weaker adsorption of Na^+ than Ca^{2+} ions in the Stern layer. Computed zeta potentials of amorphous silica also largely exceed 25.7 mV, which is the zeta potential value below where the linearized Poisson-Boltzmann equation is applicable at a temperature of 298.15 K (Eq. 2).

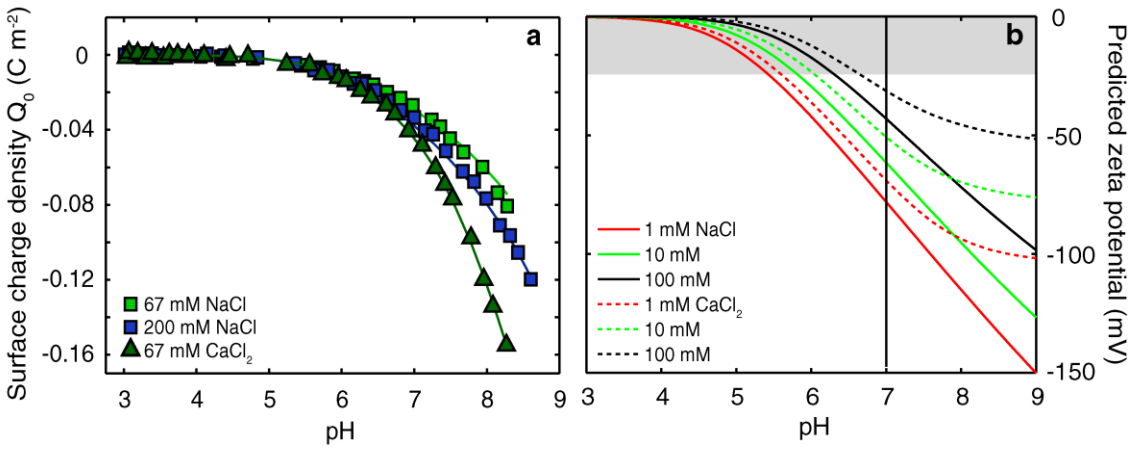

Figure 2. a: Surface charge density of amorphous silica nanoparticles (Degussa Aerosil 380 of average size 7 nm) versus pH in aqueous solutions containing NaCl or $CaCl_2$ electrolyte. The measurements from acid-base potentiometric titrations of Dove & Craven (2005) are represented by the symbols and the results of the modelling by the solid lines. **b:** Zeta potential of amorphous silica nanoparticles predicted by the basic Stern model versus pH at different NaCl and $CaCl_2$ concentrations. The gray shaded area represents electrical potentials where the linearized P-B equation is applicable ($|\varphi| \leq kT/e$ = 25.7 mV at a temperature of 298.15 K, Eq. 2).

3.1.2 Basal surface of montmorillonite

On the contrary to amorphous silica, we do not consider hydroxyl surface sites exchanging protons with the surrounding electrolyte for montmorillonite because we focus on the electrochemical properties of the basal surface, the dominating surface in terms of specific surface area and electrochemical properties (Leroy *et al.* 2007, 2017; Tournassat *et al.* 2011). The negative and permanent surface charge of the basal surface of montmorillonite originates from the isomorphic substitutions inside the crystal, for instance, the replacement of Fe^{3+} by Mg^{2+} or Fe^{2+} ions in the octahedral sheet (Grim, 1962). It is responsible for the presence of $>X^-$ surface sites that adsorb counter-ions, H^+, Na^+ or Ca^{2+} ions here, in the Stern layer (Table 3). The surface charge density of montmorillonite (Mt) was calculated according to the measured CEC (meq g^{-1}), which approximately corresponds to the negative structural charge, divided by the total specific surface area of the basal surface, SSA_b (m^2 g^{-1}), which can be given by crystallography or measured, using the following equation (Leroy *et al.* 2007; Okay *et*

al. 2014):

$$Q_0 = -\frac{e\,\mathrm{N_A}\mathrm{CEC}}{10^3 SSA_b}. \tag{20}$$

The Mt surface charge density, Q_0, was set to –0.15 C m^{-2} according to Eq. (20), using a measured CEC of 1.24 meq g^{-1} and a specific surface area of the basal surface of 750 m^2 g^{-1} (Leroy *et al.* 2015). The C_2 capacitance was set to 5.5 F m^{-2} and no C_1 capacitance was considered because no surface complexation reaction was assumed to occur at the "0-plane" (Leroy *et al.* 2007, 2015). Adsorption equilibrium constants of sodium and calcium ions in the Stern layer were directly taken from the works of Gaucher *et al.* (2009), Leroy *et al.* (2015), and Tournassat *et al.* (2016) (Table 4).

Table 3. Ion adsorption reactions on the basal surface of montmorillonite.

Surface complexation reactions	**"0-plane"**	**"β-plane"**	**Adsorption constants**
$>X^- + Na^+ \Leftrightarrow >X^- - Na^+$	0	+1	$K_{\mathrm{Mt,Na}}$
$>X^- + H^+ \Leftrightarrow >X^- - H^+$	0	+1	$K_{\mathrm{Mt,H}}$
$2>X^- + Ca^{2+} \Leftrightarrow >X_2Ca$	0	+2	$K_{\mathrm{Mt,Ca}}$

Table 4. Parameters of the extended Stern model for the basal surface of montmorillonite.

Parameters	**Values**
Surface charge density Q_0 (C m^{-2})	–0.15 [1]
Log(Na^+ adsorption constant) Log$K_{\mathrm{Mt,Na}}$	0.05 [2]
Log(H^+ adsorption constant) Log$K_{\mathrm{Mt,H}}$	0.55 [3]
Log(Ca^{2+} adsorption constant) Log$K_{\mathrm{Mt,Ca}}$	0.7 [4]
Outer capacitance C_2 (F m^{-2})	5.5 [1]

[1] From Eq. (20).
[2] From Leroy *et al.* (2015) according to electrophoretic mobility measurements and molecular dynamics simulations (Sondi *et al.* 1996; Tournassat *et al.* 2009; Bourg & Sposito 2011).
[3] From Leroy *et al.* (2015) and Tournassat *et al.* (2016) using $K_{\mathrm{Mt,H}} = K_{\mathrm{Mt,Na}}K_{\mathrm{Mt,NaH}}$ with $K_{\mathrm{Mt,NaH}} = 10^{0.5}$ for the exchange of adsorbed Na^+ by H^+ ion.
[4] From Leroy *et al.* (2015) and Gaucher *et al.* (2009) using $K_{\mathrm{Mt,Ca}} = K_{\mathrm{Mt,Na}}^2K_{\mathrm{Mt,NaCa}}$ with $K_{\mathrm{Mt,NaCa}} = 10^{0.6}$ for the exchange of adsorbed Na^+ by Ca^{2+} ion.
Note that $>X^-$ surface site represents the negative surface site arising from isomorphic

substitutions in the crystal of montmorillonite; $2{>}X^-$ means that there are two $>X^-$ surface sites.

Finally, the approach of Leroy *et al.* (2007) was used to compute the negative zeta potential of the basal surface of montmorillonite at pH = 7 (neutral condition) as a function of NaCl or $CaCl_2$ concentration in the salinity range 1 to 100 mM (more details on the calculation procedure is given in Leroy *et al.* 2007) (Fig. 3). As in the case of amorphous silica, predicted zeta potential increases in magnitude when salinity decreases, especially for NaCl electrolyte because of weaker adsorption of Na^+ than Ca^{2+} ions in the Stern layer (Table 4). Computed zeta potentials also largely exceed 25.7 mV.

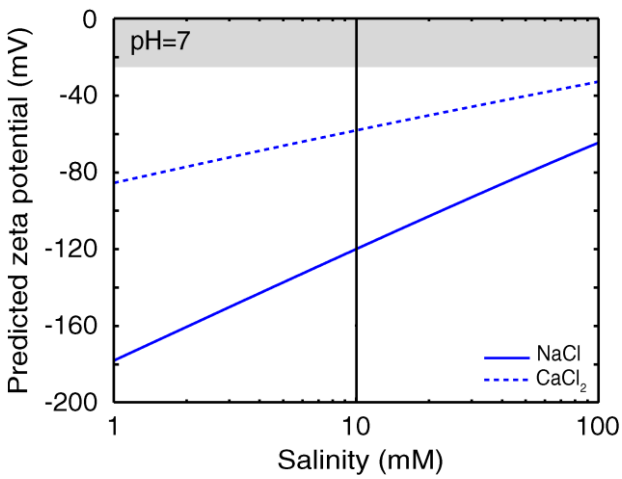

Figure 3. Zeta potential of the basal surface of montmorillonite predicted by the extended Stern model versus concentration of NaCl or $CaCl_2$ electrolyte at pH = 7. The gray shaded area represents electrical potentials where the linearized P-B equation is applicable ($|\varphi| \leq kT/e$ = 25.7 mV at a temperature of 298.15 K, Eq. 2).

3.2 Electrical potential profiles

The main output of the surface complexation modelling is the ζ-potential (as function of pH and salinity) associated to the considered system. Its values for amorphous silica (pH = 7 and pH = 9) and the basal surface of montmorillonite (pH = 7) in contact with NaCl or $CaCl_2$ electrolyte are reported in Table 5. The so-determined

values of the ζ-potential are then used as input to solve the full P-B equation (Eqs. 12-15). We took two different pH for amorphous silica because of its surface charge becoming more negative when pH increases (Fig. 2a).

Table 5. Zeta potentials (ζ) of amorphous silica and basal surface of montmorillonite computed from our surface complexation models.

Salinities (mM)	**NaCl**			**$CaCl_2$**		
	1	**10**	**100**	**1**	**10**	**100**
Amorphous silica ζ (mV) at pH = 7	–82.1	–62.3	–43.1	–71.3	–51.0	–31.4
Amorphous silica ζ (mV) at pH = 9	–153.9	–127.8	–98.5	–102.1	–76.2	–51.6
Montmorillonite ζ (mV) at pH = 7	–178.0	–120.0	–64.6	–85.5	–58.1	–32.8

We also defined another parameter, Ω, to characterize the thickness of fully developed diffuse layer, Δ, relative to the cylinder radius:

$$\Omega = \frac{\Delta}{r_0}, \tag{21}$$

where $\Delta = 5\chi$ (Manciu & Ruckenstein 2003; Leroy *et al.* 2010, 2015). Debye lengths, χ, computed as a function of salt concentration (Eq. 5) and ratios between diffuse layer thickness and r_0 (Eq. 21) are reported in Table 6. Our calculations show that overlapping diffuse layers may appear for salinities of 1 and 10 mM NaCl and $CaCl_2$ and 100 mM NaCl when r_0 = 5 nm and for 1 mM NaCl when r_0 = 50 nm because $\Omega \sim 1$ and $\Omega > 1$.

Table 6. Debye lengths and ratios of thickness of diffuse layer to cylinder radius computed as a function of salt concentration (T = 298.15 K) (Eqs. 5 and 21).

Salt concentration (mM)	**1**	**10**	**100**
χ_{NaCl} (nm)	9.61	3.04	0.96
χ_{CaCl_2} (nm)	5.55	1.76	0.56

Ω_{NaCl} ($r_0 = 5$ nm)	9.61*	3.04*	0.96*
Ω_{CaCl_2} ($r_0 = 5$ nm)	5.55*	1.76*	0.56
Ω_{NaCl} ($r_0 = 50$ nm)	0.96*	0.30	0.10
Ω_{CaCl_2} ($r_0 = 50$ nm)	0.56	0.18	0.06
Ω_{NaCl} ($r_0 = 500$ nm)	0.10	0.03	0.01
Ω_{CaCl_2} ($r_0 = 500$ nm)	0.06	0.02	0.01

* Diffuse layer overlapping.

Results of the modelling for a cylinder of radius $r_0 = 5$ nm are presented in Fig. 4 (amorphous silica) and Fig. 5 (montmorillonite). The linearized P-B equation significantly overestimates the electrical potential computed from the full P-B equation, except when the salinity is high (100 mM), because of the high zeta potential magnitudes and interacting diffuse layers. Observed effect increases when salinity decreases and pH increases for amorphous silica, and is particularly strong when calcium ion is in solution because of the approximation $\varphi << kT/(2e) \cong 12.8$ mV for Ca^{2+} (Debye-Hückel approximation of the Poisson-Boltzmann equation, Eq. 2). Note that the Matlab computations for the full P-B equation were checked using a partial differential equations (PDE) solver based on the finite-element method (the Electrostatics module of COMSOL Multiphysics™ 3.5).

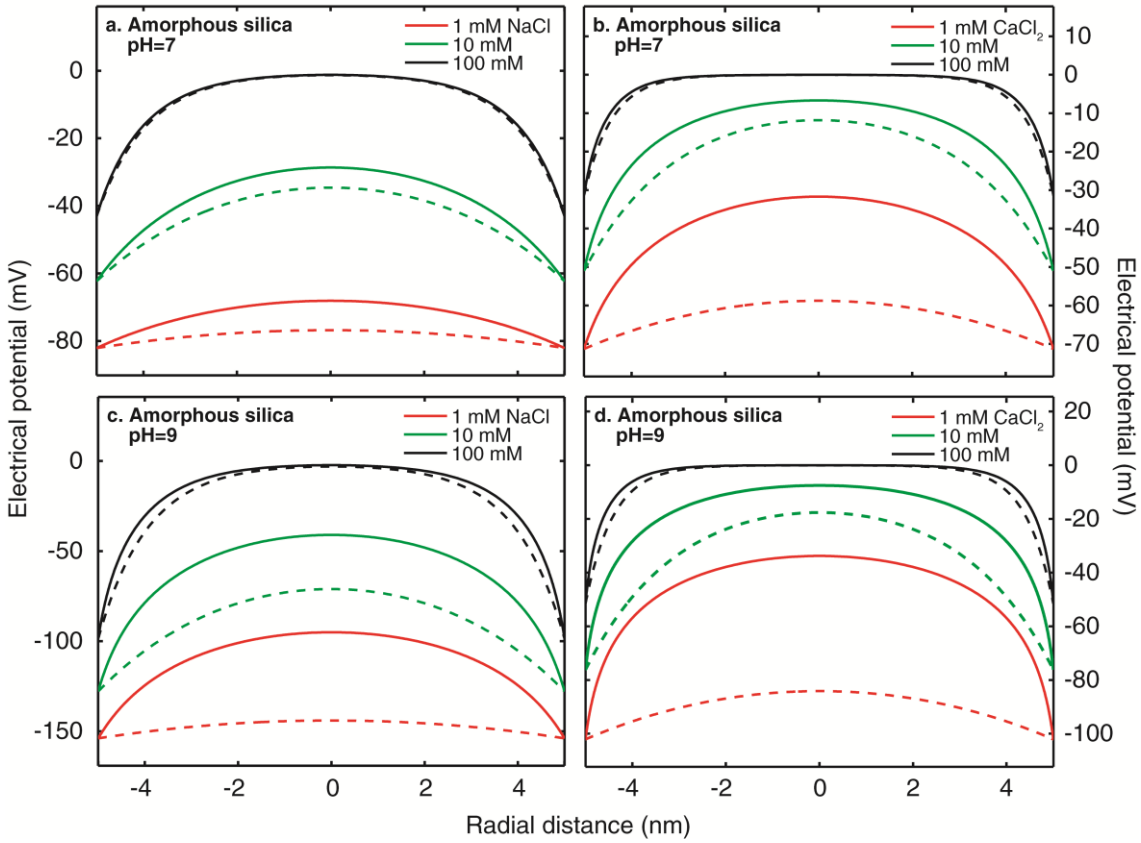

Figure 4. Electrical potential profiles in amorphous silica nanotubes computed from our code (full P-B equation) (solid lines) and the linearized P-B equation (dashed lines) (r_0 = 5 nm).

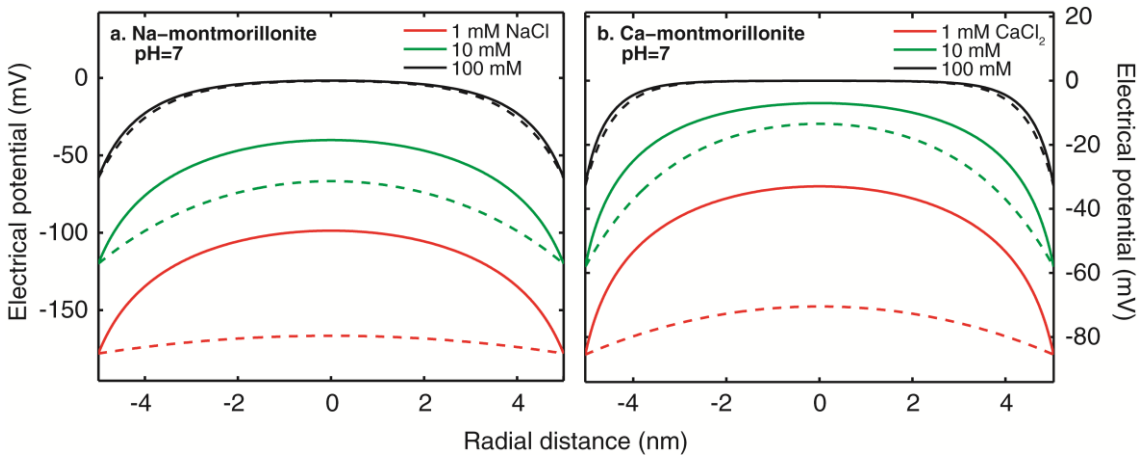

Figure 5. Electrical potential profiles in montmorillonite nanotubes computed from our code (full P-B equation) (solid lines) and the linearized P-B equation (dashed lines) (r_0 = 5 nm).

When the radius of the cylinder increases from 5 to 50 nm, the linearized P-B equation only significantly overestimates the electrical potential computed from the full

P-B equation when the salinity of the electrolyte is very low (1 mM) because of the high magnitude of the zeta potential (Fig. 6 and Fig. 7). At the center of the pore, the electrical potential is not significantly overestimated because the electroneutrality condition nearly occurs (1 mM NaCl) or applies (other salinities).

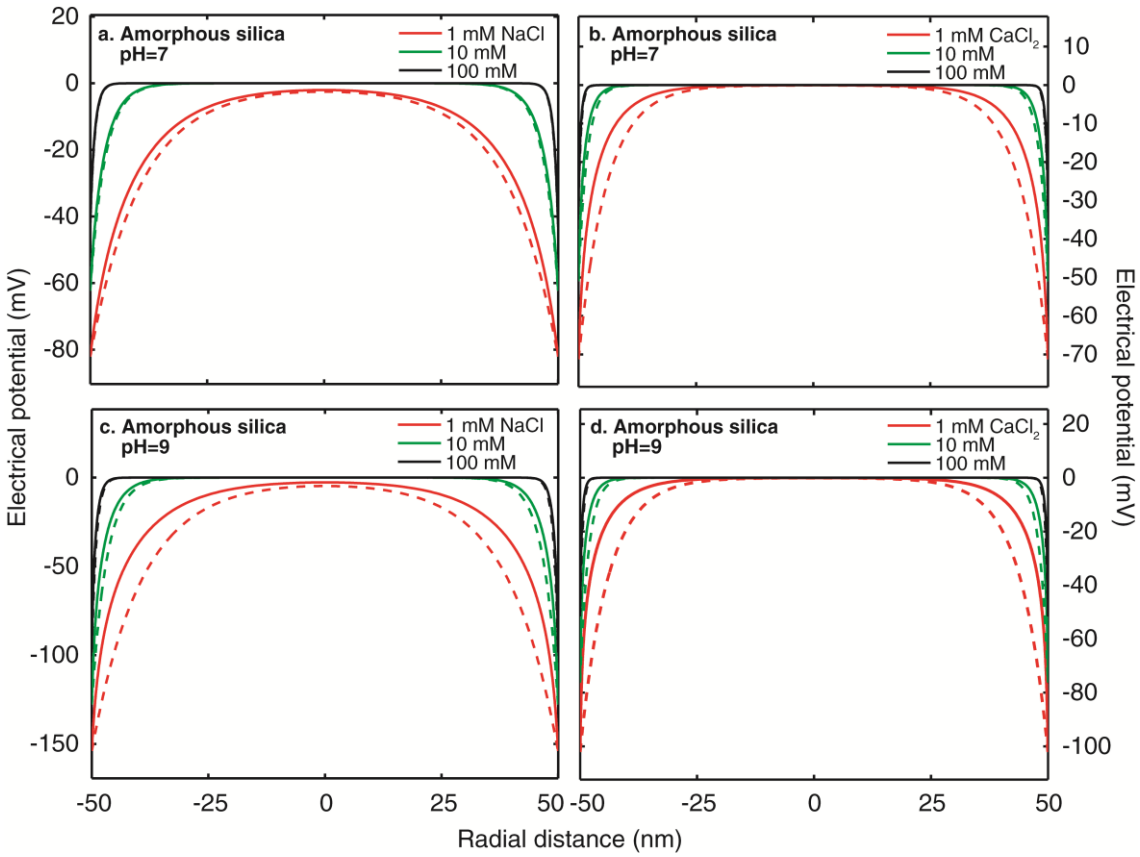

Figure 6. Electrical potential profiles in amorphous silica nanotubes computed from our code (full P-B equation) (solid lines) and the linearized P-B equation (dashed lines) (r_0 = 50 nm).

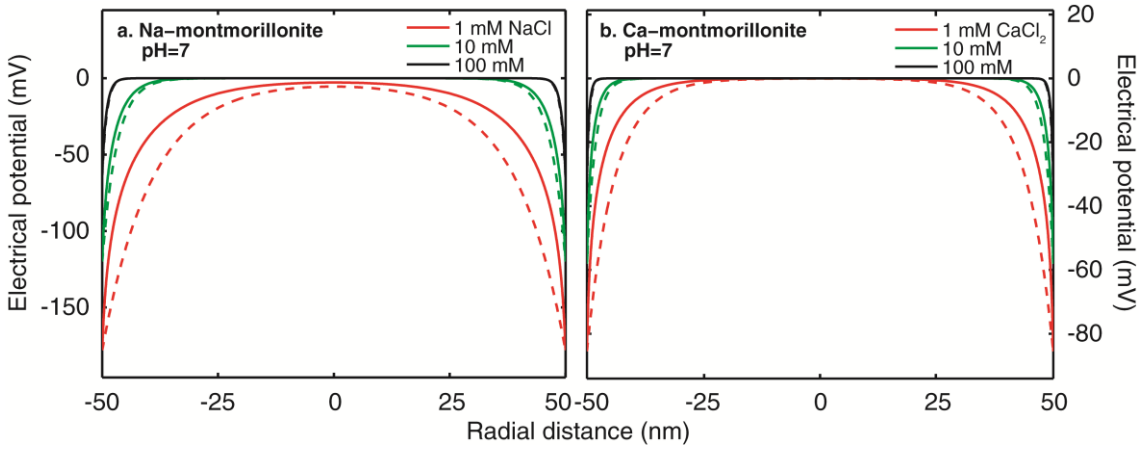

Figure 7. Electrical potential profiles in montmorillonite nanotubes computed from our code (full P-B equation) (solid lines) and the linearized P-B equation (dashed lines) (r_0 = 50 nm).

When the radius of the cylinder is 500 nm, the electroneutrality condition is always respected in the bulk electrolyte at the center of the pore. Nevertheless, the electrical potential calculated from the full P-B equation is still overestimated by the linearized P-B equation when zeta potential is high, especially for $CaCl_2$ electrolyte (Fig. 8 and Fig. 9).

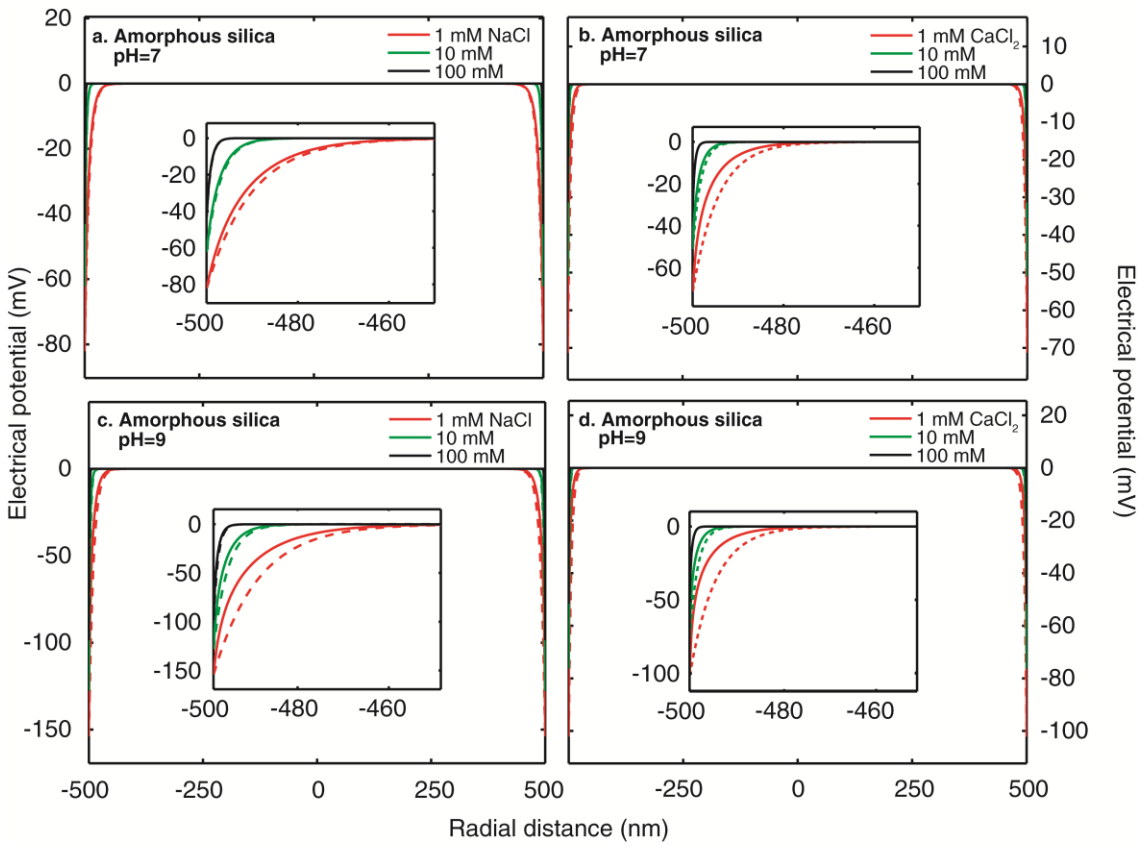

Figure 8. Electrical potential profiles in amorphous silica nanotubes computed from our code (full P-B equation) (solid lines) and the linearized P-B equation (dashed lines) (r_0 = 500 nm).

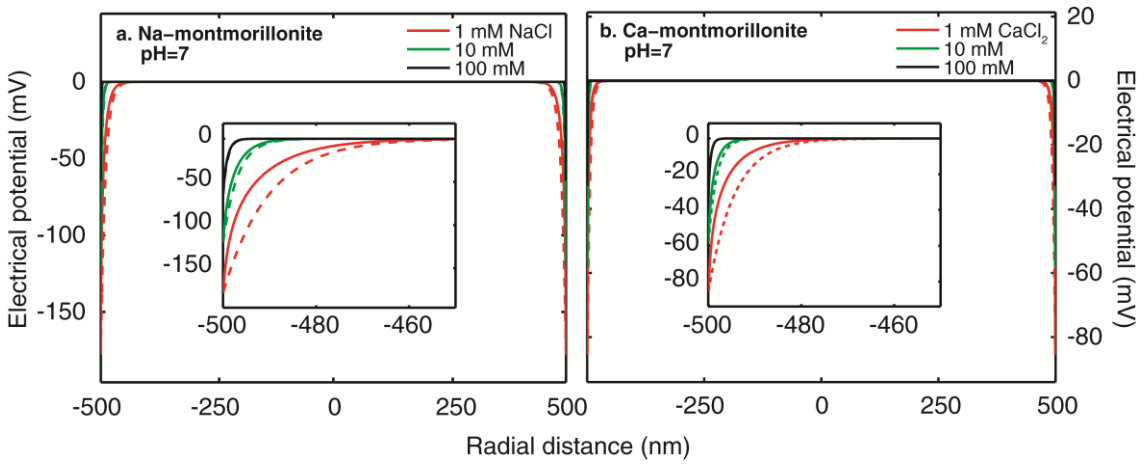

Figure 9. Electrical potential profiles in montmorillonite nanotubes computed from our code (full P-B equation) (solid lines) and the linearized P-B equation (dashed lines) (r_0 = 500 nm).

Our calculations show that the linearized P-B equation may overestimate the electrical potential predicted by the full P-B equation for highly charged nanocylinders.

For such nanopores, the P-B equation may also have some shortcomings such as not considering the fine size of the ion, specific ion-surface interactions, attractive ion-ion interactions and ion-ion correlations (Borukhov *et al.* 1997; Wernersson *et al.* 2010; Bonthuis & Netz 2013). Despite these shortcomings, the P-B equation is still widely used because it can describe the electrostatic behaviors of most charged systems when surfaces are separated by a distance superior to 5 nm (Montes Ruiz-Cabello *et al.* 2014). Its relative simplicity makes it more useable than more elaborate theories, which need more parameters and do not necessarily agree with each other (Vlachy 1999; Grochowski & Trylska 2008; Ben-Yaakov *et al.* 2009; López-García *et al.* 2014). There is still not a universal theory supplanting the P-B equation to describe ion and water distribution at interfaces. Furthermore, our improved electrical potential profiles compared to those from the linearized P-B equation must be considered with caution because of the assumptions inherent to water flow and solute transport modelling at the macroscopic (laboratory) scale. Considering for instance pores as cylinders and the upscaling procedure of the model predictions to the laboratory scale may also bring some significant uncertainties that render the improvement considering the full P-B equation more negligible when simulating the electrical properties of charged materials at the macroscopic scale.

4. CONCLUSIONS AND PROSPECTS

We have developed a short Matlab® code to numerically solve the Poisson-Boltzmann equation inside a charged cylinder filled by an electrolyte containing any type of ions. The input parameters of our code are the zeta potential and the chemical composition of the bulk electrolyte. Unlike the linearized P-B equation with the Debye-Hückel approximation, our code is not limited to low zeta potentials of magnitude

inferior to 25.7 mV at a temperature of 25 °C.

We applied our code to simulate the electrochemical properties of amorphous silica and montmorillonite nanotubes containing a NaCl or $CaCl_2$ aqueous electrolyte. For that purpose, the zeta potentials were computed using well-established surface complexation models that consider the Stern and diffuse layer at the surface of the mineral. We show that the electrical potential inferred from the full P-B equation is overestimated by the linearized P-B equation when the zeta potentials are high (above 25.7 mV at a temperature of 25 °C) and the cylinder radius goes to the nm range where diffuse layers may overlap, especially for $CaCl_2$ electrolyte. Diffuse layers overlap when the cylinder radius is smaller or equal to approximately five Debye lengths, which correspond for instance to approximately 50, 15 nm and 30, 10 nm for respectively 1, 10 mM NaCl and $CaCl_2$ at a temperature of 25 °C. Underground, these conditions typically occur for highly charged nanopores containing a dilute aqueous electrolyte (ionic strength < 0.1 M) such as those of clays and low-pH cements.

As a perspective, it would be very interesting to combine our P-B code with transport codes in electrokinetics and hydrogeophysics that consider the electrochemical properties of charged cylinders (Daiguji 2010; Jougnot *et al.* 2012; Bücker & Hördt 2013a). Compared to the use of the linearized P-B equation, this combination would improve, for instance, the simulation of electro-osmosis in highly charged nanopores in nanofluidics and of the self-potential and complex conductivity response of clayey rocks and low-pH cements in hydrogeophysics. In addition, to better describe interacting diffuse layers, it would be relevant to modify our P-B code to consider as input parameter the surface charge density instead of the zeta potential.

ACKNOWLEDGMENTS

The authors sincerely thank the Associate Editor, Gary Egbert, and the two reviewers, Andreas Hördt and Matthias Bücker, for helping them to significantly improve the quality of the manuscript. The work of P. Leroy was funded by the Horizon 2020 CEBAMA (Contract Number: 662147), Andra UP-Transfert (coordinated by Pierre Henocq) and NEEDS (Zetaclay and TRANSREAC) projects. A. Maineult acknowledges the support of the Russian Science Foundation (Grant No. 17-17-01160 'Physical-chemical models of Induced Polarization and Self-Potential with application to pumping test experiments'). Philippe Leroy warmly thanks Francis Claret for his support and Christophe Tournassat for fruitful discussions.

Appendix A: origins of the Poisson-Boltzmann equation

The P-B equation is derived from the works of Poisson (1824) for the electrical potential and Boltzmann (1909) for the ion distributions at the interface between two phases such as mineral and water. In electrostatics, Poisson's equation is derived from the differential form of Gauss' law, which describes the divergence of the dielectric displacement **D** due to the volumetric charge density ρ of the medium (C m^{-3}) (Hunter 1981):

$$\nabla \bullet \mathbf{D} = \rho . \tag{A1}$$

The dielectric displacement is:

$$\mathbf{D} = \varepsilon \mathbf{E}, \tag{A2}$$

where **E** is the electrical field (V m^{-1}), which is defined by:

$$\mathbf{E} = -\nabla \varphi . \tag{A3}$$

Eq. (A2) shows that the effect of the electrical field on the dielectric displacement is weighted by the dielectric permittivity, which measures the capacity of a solvent to affect the electrical field strength, i.e. the capacity of the molecular dipoles to align themselves to cancel part of the electrical field.

The Poisson equation is obtained by combining Eqs. (A1) to (A3) and assuming that the dielectric permittivity of the solvent is constant (Hunter 1981). This yields:

$$\nabla^2 \varphi = -\frac{\rho}{\varepsilon} . \tag{A4}$$

The volumetric charge density is:

$$\rho = \sum_{i=1}^{M} q_i 1000 \, \mathrm{N_A} \, C_i^{\alpha} , \tag{A5}$$

where C_i^{α} is the ion concentration, for instance, at the interface between two phases such as mineral and water. Eq. (A5) shows that it is necessary to know C_i^{α} to solve the

Poisson equation for the electrostatic potential φ.

Boltzmann (1909) showed that it is possible to relate the ion concentration to the electrostatic potential at the interface when the medium is in or close to thermodynamic equilibrium. In that case, the chemical potentials μ (J) of the ion and solvent are the same at the interface and in the bulk solution (Lyklema 1995; Revil & Leroy 2004). This yields for the chemical potentials of the ion:

$$\mu_i^{\alpha} = \mu_i \,, \tag{A6}$$

which are written as according to thermodynamics (Lyklema 1995):

$$\mu_i^{\alpha} = \mu_i^{\alpha,R} + kT \ln a_i^{\alpha} + q_i \varphi \,, \tag{A7}$$

$$\mu_i = \mu_i^{R} + kT \ln a_i \,, \tag{A8}$$

where the superscript R for the chemical potentials corresponds to the reference (standard) state, which is the point of zero charge for the interface (Sverjensky 2005) and the unit molar concentration of the ion at hypothetical infinite dilution for the bulk solution (Lyklema 1995). The quantity a_i is the activity coefficient of the ion (dimensionless), which is written as:

$$a_i = \gamma_i \frac{C_i}{C_0} \,, \tag{A9}$$

where γ_i and C_0 are respectively the ion activity coefficient (dimensionless) and standard molarity (1 mol L^{-1}). The Boltzmann equation is obtained by combining Eqs. (A6)-(A9), considering $\mu_i^{\alpha,R} = \mu_i^{R}$ and the same ion activity coefficient in the interface and bulk electrolyte ($\gamma_i^{\alpha} = \gamma_i$). This yields:

$$C_i^{\alpha} = C_i \exp\left(-\frac{q_i \varphi}{kT}\right) \,, \tag{A10}$$

where C_i is the ionic concentration in the bulk electrolyte. The P-B equation is finally

obtained by combining Eqs. (A4), (A5) and (A10), yielding:

$$\nabla^2\varphi = -\frac{1000\,\mathrm{N_A}}{\varepsilon}\sum_{i=1}^{M} q_i C_i \exp\left(-\frac{q_i\varphi}{kT}\right). \tag{A11}$$

Appendix B: the Matlab® code

Our numerical solution of the P-B equation is based on the Matlab® bvp4c function for solving boundary value problems. For implementation, Eq. (13) is rewritten as:

$$\begin{cases} y_1' = y_2 \\ y_2' = -\dfrac{1}{R} y_2 - \dfrac{\sum_{i=1}^{M} s_i C_i \exp\left(-s_i y_1\right)}{\sum_{i=1}^{M} s_i^2 C_i} \end{cases} . \tag{B1}$$

The term with the sums has to be defined as a singular term in bvp4c. The boundary conditions (14) and (15) become:

$$\begin{cases} y_1\left(R_0\right) = \xi \\ y_2\left(0\right) = 0 \end{cases} . \tag{B2}$$

The main program is:

```
clear all
close all
fclose all;

global s C xsi S

elementary_charge=1.6021766208e-19;
k=1.38064852e-23;
NA=6.022140857e23;
epsilon0=8.854187e-12;

TC=input('temperature (°C, between 2 and 87°C): ');
T=273.15+TC;

a0=87.8950234752; % From Lide, D.R., 1990. CRC Handbook of Chemistry and
a1=-0.4002899766;  % Physics, CRC Press, Boca Raton, p. 6-15
a2=0.0008613222;
a3=-0.0000009565;

epsilon=(a3*TC^3+a2*TC^2+a1*TC+a0)*epsilon0;

r0=input('radius of the cylinder (µm): ');
r0=r0*1e-6; % radius in meter

zeta=input('zeta potential (mV): ');
zeta=zeta/1000; % zeta in V

M=input('number of ionic species: ');
for i=1:M
   disp(['ion type n° ',num2str(i),': '])
   s(i)=input('  sign of the charge x valence: ');
   C(i)=input('  concentration (mol/L): ');
   C(i)=C(i)*1000; % concentration in mol/m3
```

```
end

S=1/sum(s.^2.*C);
Debye=sqrt(epsilon*k*T/(elementary_charge^2*NA*sum(s.^2.*C)));
R0=r0/Debye;
xsi=elementary_charge/k/T*zeta;

[R,P]=f_PBE_solve(R0);

r=R*Debye;
potential=P/elementary_charge*k*T;

figure (1)
   plot(r*1e6,potential*1000,'r-','LineWidth',2)
   xlabel('radial distance (µm)')
   ylabel('potential (mV)')
   box on
```

The input parameters are the radius r_0 (µm), the zeta-potential ζ (mV), the number of ionic species M, the sign of the charge times the valence s_i and the concentration C_i (mol L^{-1}) for each ion type. Note that the water temperature can also be changed in the program for a temperature between 2 and 87 °C. The dielectric permittivity of water is calculated according to the measurements reported in Lide (1990) at a pressure of one bar. In addition, to correctly solve the P-B equation, the bulk electrolyte must be electroneutral (the chemical composition must satisfy Eq. (3)).

The function f_PBE_solve is:

```
function [R,P]=f_PBE_solve(R0)
global xsi

% Singular term
S=[0,0;0,-1];
options=bvpset('SingularTerm',S,'Nmax',250000,'RelTol',1e-12);

% Initial solution
solinit=bvpinit(linspace(0,R0,1000),[0 xsi]);

% Solution
sol=bvp4c(@f_PBEmts,@f_BCPBE,solinit,options);

R=sol.x;
P=sol.y(1,:);
```

Note that the initial solution (defined using bvpinit) is a vector of size 1000. This size

should sometimes be increased if the code is unable to compute the Jacobian properly.

The function f_PBEmts is:

```
function dydx=f_PBEmts(x,y)
global s C S

dydx=[y(2);-sum(s.*C.*exp(-s.*y(1)))*S];
```

And the function f_BCPBE is:

```
function y=f_BCPBE(ya,yb)
global xsi

y=[ya(2);yb(1)-xsi];
```

References

Bairlein, K., Bücker, M., Hördt, A. & Hinze, B., 2016. Temperature dependence of spectral induced polarization data: experimental results and membrane polarization theory, *Geophys. J. Int.*, **205**(1), 440–453.

Ben-Yaakov, D., Andelman, D., Harries, D. & Podgornik, R., 2009. Beyond standard Poisson–Boltzmann theory: ion-specific interactions in aqueous solutions, *J. Phys. Condens. Matter*, **21**(42), 424106, doi: 10.1088/0953-8984/21/42/424106.

Bernabé, Y., 1998. Streaming potential in heterogeneous networks, *J. Geophys. Res. Solid Earth*, **103**(B9), 20,827–20,841.

Bocquet, L. & Charlaix, E., 2010. Nanofluidics, from bulk to interfaces, *Chem. Soc. Rev.*, **39**, 1073–1095.

Boltzmann, L., 1909. Wissenschaftliche Abhandlungen. Cambridge University Press.

Bonthuis, D.J. & Netz, R.R., 2013. Beyond the Continuum: How Molecular Solvent Structure Affects Electrostatics and Hydrodynamics at Solid-Electrolyte Interfaces, *J. Phys. Chem. B*, **117**, 11,397–11,413.

Borukhov, I., Andelman, D. & Orland, H., 1997. Steric effects in electrolytes: A modified Poisson-Boltzmann equation, *Phys. Rev. Lett.*, **79**, 435–438.

Bourg, I.C., Sposito, G. & Bourg, A.C.M., 2007. Modeling the acid-base surface chemistry of montmorillonite, *J. Colloid Interface Sci.*, **312**, 297–310.

Bourg, I.C., Sposito, G., 2011. Molecular dynamics simulations of the electrical double layer on smectite surfaces contacting concentrated mixed electrolyte (NaCl-$CaCl_2$) solutions, *J. Colloid Interface Sci.*, **360**, 701–715.

Bücker, M. & Hördt, A., 2013a. Analytical modelling of membrane polarization with explicit parametrization of pore radii and the electrical double layer, Geophys. J. Int., **194**(2), 804–813.

Bücker, M. & Hördt, A., 2013b. Long and short narrow pore models for membrane polarization, *Geophysics*, **78**(6), E299–E314.

Caceci, M. & Cacheris, W.P., 1984. Fitting curves to data. The Simplex algorithm is the answer, Byte, **9**, 340–362.

Chapman, D.L., 1913. A contribution to the theory of electrocapillarity. *The London, Edinburgh and Dublin Philos. Mag. J. Sci. series 6*, **25**, 475–481.

Chuprinko, D. & Titov, K., 2017. Influence of mineral composition on spectral induced polarization in sediments, *Geophys. J. Int.*, **209**(1), 186–191.

Conlisk, A.T., 2005. The Debye-Hückel approximation: Its use in describing electroosmotic flow in micro- and nanochannels, *Electrophoresis*, **26**, 1896–1912.

Daiguji, H., 2010. Ion transport in nanofluidic channels, *Chem. Soc. Rev.*, **39**, 901–911.

Davis, J.A., James, R.O. & Leckie, J.O., 1978. Surface Ionization and Complexation at Oxide-Water Interface .1. Computation of Electrical Double-Layer Properties in Simple Electrolytes, *J. Colloid Interface Sci.*, **63**, 480–499.

Delgado, A.V., Gonzalez-Caballero, F., Hunter, R.J., Koopal, L.K. & Lyklema, J., 2007. Measurement and interpretation of electrokinetic phenomena, *J. Colloid Interface Sci.*, **309**, 194–224.

Dove, P.M. & Craven, C.M., 2005. Surface charge density on silica in alkali and alkaline earth chloride electrolyte solutions, *Geochim. Cosmochim. Acta*, **69**, 4963–4970.

Dufreche, J.F., Marry, V., Bernard, O. & Turq, P., 2001. Models for electrokinetic phenomena in montmorillonite, *Colloids Surf., A Physicochem. Eng. Asp.*, **195**, 171–180.

Dufreche, J.F., Marry, V., Malikova, N. & Turq, P., 2005. Molecular hydrodynamics for

electro-osmosis in clays: from Kubo to Smoluchowski, *J. Mol. Liq.*, **118**, 145–153.

Gaucher, E.C., Tournassat, C., Pearson, F.J., Blanc, P., Crouzet, C., Lerouge, C. & Altmann, S., 2009. A robust model for pore-water chemistry of clayrock, *Geochim. Cosmochim. Acta*, **73**, 6470–6487.

Gouy, G., 1910. Sur la constitution de la charge électrique a surface d'un électrolyte, *J. Phys. Theor. Appl.*, **9**(1), 457-468.

Grangeon, S., Claret, F., Lerouge, C., Warmont, F., Sato, T., Anraku, S., Numako, C., Linard, Y. & Lanson, B., 2013. On the nature of structural disorder in calcium silicate hydrates with a calcium/silicon ratio similar to tobermorite, *Cem. Concr. Res.*, **52**, 31–37.

Grim, R.E., 1962. Applied Clay Mineralogy. McGraw–Hill, New York.

Grochowski, P. & Trylska, J., 2008. Continuum molecular electrostatics, salt effects, and counterion binding—A review of the Poisson–Boltzmann theory and its modifications, *Biopolymers*, **89**, 93–113.

Heuser, M., Spagnoli, G., Leroy, P., Klitzsch, N. & Stanjek, H., 2012. Electro-osmotic flow in clays and its potential for reducing clogging in mechanical tunnel driving, *Bull. Eng. Geol. Environ.*, **71**, 721–733.

Hiemstra, T., De Wit, J.C.M. & Van Riemsdijk, W.H., 1989. Multisite proton adsorption modelling at the solid/solution interface of (hydr)oxides: a new approach. II. Application to various important (hydr)oxides, *J. Colloid Interface Sci.*, **133**, 105–117.

Hördt, A., Bairlein, K., Bielefeld, A., Bücker, M., Kuhn, E., Nordsiek, S. & Stebner, H., 2016. The dependence of induced polarization on fluid salinity and pH, studied with an extended model of membrane polarization, *J. Appl. Geophys.*, **135**, 408–

417.

Hördt, A., Bairlein, K., Bücker, M. & Stebner, H., 2017. Geometrical constraints for membrane polarization, *Near Surface Geophys.*, **15**(6), 579–592.

Hunter, R.J., 1981. Zeta Potential in Colloid Science: Principles and Applications. Academic Press, New York.

Jougnot, D., Linde, N., Revil, A. & Doussan, C., 2012. Derivation of Soil-Specific Streaming Potential Electrical Parameters from Hydrodynamic Characteristics of Partially Saturated Soils, *Vadose Zone J.*, 11, doi: 10.2136/vzj2011.0086.

Kruschwitz, S., Prinz, C. & Zimathies, A., 2016. Study into the correlation of dominant pore throat size and SIP relaxation frequency, *J. Appl. Geophys.*, **135**, 375–386.

Labbez, C., Jonsson, B., Pochard, I., Nonat, A. & Cabane, B., 2006. Surface charge density and electrokinetic potential of highly charged minerals: Experiments and Monte Carlo simulations on calcium silicate hydrate, *J. Phys. Chem. B*, **110**, 9219–9230.

Lerouge, C., Gaboreau, S., Grangeon, S., Claret, F., Warmont, F., Jenni, A., Cloet, V. & Mäder, U., 2017. In situ interactions between Opalinus Clay and Low Alkali Concrete, *Phys. Chem. Earth, Parts A/B/C*, **99**, 3–21.

Leroy, P. & Revil, A., 2004. A triple-layer model of the surface electrochemical properties of clay minerals, *J. Colloid Interface Sci.*, **270**, 371–380.

Leroy, P., Revil, A., Altmann, S. & Tournassat, C., 2007. Modeling the composition of the pore water in a clay-rock geological formation (Callovo-Oxfordian, France), *Geochim. Cosmochim. Acta*, **71**, 1087–1097.

Leroy, P., Revil, A., Kemna, A., Cosenza, P. & Ghorbani, A., 2008. Complex conductivity of water-saturated packs of glass beads, *J. Colloid Interface Sci.*, **321**, 103–117.

Leroy, P., Lassin, A., Azaroual, M. & Andre, L., 2010. Predicting the surface tension of aqueous 1:1 electrolyte solutions at high salinity, *Geochim. Cosmochim. Acta*, **74**, 5427–5442.

Leroy, P., Jougnot, D., Revil, A., Lassin, A. & Azaroual, M., 2012. A double layer model of the gas bubble/water interface, *J. Colloid Interface Sci.*, **388**, 243–256.

Leroy, P., Devau, N., Revil, A. & Bizi, M., 2013. Influence of surface conductivity on the apparent zeta potential of amorphous silica nanoparticles, *J. Colloid Interface Sci.*, **410**, 81–93.

Leroy, P., Tournassat, C., Bernard, O., Devau, N. & Azaroual, M., 2015. The electrophoretic mobility of montmorillonite. Zeta potential and surface conductivity effects, *J. Colloid Interface Sci.*, **451**, 21–39.

Leroy, P., Weigand, M., Mériguet, G., Zimmermann, E., Tournassat, C., Fagerlund, F., Kemna, A. & Huisman, J.A., 2017. Spectral induced polarization of Na-montmorillonite dispersions, *J. Colloid Interface Sci.*, **505**, 1093–1110.

Li, S., Raoof, A. & Schotting, R., 2014. Solute dispersion under electric and pressure driven flows; pore scale processes, *J. Hydrol.*, **517**, 1107–1113.

Li, S., Leroy, P., Heberling, F., Devau, N., Jougnot, D. & Chiaberge, C., 2016. Influence of surface conductivity on the apparent zeta potential of calcite, *J. Colloid. Interface Sci.*, 468, 262–275.

Lide, D.R., 1990. CRC Handbook of Chemistry and Physics CRC Press, Boca Raton.

López-García, J.J., Horno, J. & Grosse, C., 2014. Influence of the finite size and effective permittivity of ions on the equilibrium double layer around colloidal particles in aqueous electrolyte solution, *J. Colloid Interface Sci.*, **428**, 308–315.

Lyklema, J., 1995. Fundamentals of Interface and Colloid Science. Volume II: Solid-Liquid Interfaces. Academic Press, London.

Lyklema, J., Rovillard, S. & De Coninck, J., 1998. Electrokinetics: The properties of the stagnant layer unraveled, *Langmuir*, **14**, 5659–5663.

Malusis, M.A., Shackelford, C.D. & Olsen, H.W., 2003. Flow and transport through clay membrane barriers, *Eng. Geol.*, **70**, 235–248.

Manciu, M. & Ruckenstein, E., 2003. Specific ion effects via ion hydration: I. Surface tension, *Adv. Colloid Interface Sci.*, **105**, 63–101.

McCleskey, R.B., 2011. Electrical Conductivity of Electrolytes Found In Natural Waters from (5 to 90) degrees C, *J. Chem. Eng. Data*, **56**, 317–327.

Montes Ruiz-Cabello, F.J., Trefalt, G., Maroni, P. & Borkovec, M., 2014. Accurate Predictions of Forces in the Presence of Multivalent Ions by Poisson–Boltzmann Theory, *Langmuir*, **30**, 4551–4555.

Obliger, A., Jardat, M., Coelho, D., Bekri, S. & Rotenberg, B., 2014. Pore network model of electrokinetic transport through charged porous media, *Phys. Rev. E*, **89,** 043013, doi: 10.1103/PhysRevE.89.043013

Okay, G., Leroy, P., Ghorbani, A., Cosenza, P., Camerlynck, C., Cabrera, J., Florsch, N. & Revil, A., 2014. Spectral induced polarization of clay-sand mixtures: Experiments and modeling, *Geophysics*, **79**(6), E353–E375.

Poisson, S.D., 1824. Mémoire Sur La Théorie Du Magnétisme. Mémoires de l'Académie des Sciences de l'Institut de France, Paris.

Pride, S., 1994. Governing Equations for the Coupled Electromagnetics and Acoustics of Porous-Media, *Phys. Rev. B*, **50**, 15,678–15,696.

Rasmusson, M., Rowlands, W., O'Brien, R.W. & Hunter, R.J., 1997. The dynamic mobility and dielectric response of sodium bentonite, *J. Colloid Interface Sci.*, **189**, 92–100.

Revil, A. & Leroy, P., 2004. Constitutive equations for ionic transport in porous shales.

J. Geophys. Res. Solid Earth, **109**(B3), B03208, doi: 10.1029/2003JB002755.

Revil, A. & Florsch, N., 2010. Determination of permeability from spectral induced polarization in granular media, *Geophys. J. Int.*, **181**(3), 1480–1498.

Revil, A., Koch, K. & Holliger, K., 2012. Is it the grain size or the characteristic pore size that controls the induced polarization relaxation time of clean sands and sandstones?, *Water Resour. Res.*, **48**(5), W05602, doi: 10.1029/2011WR011561.

Revil, A., Binley, A., Mejus, L. & Kessouri, P., 2015. Predicting permeability from the characteristic relaxation time and intrinsic formation factor of complex conductivity spectra, *Water Resour. Res.*, **51**(8), 6672–6700.

Rotenberg, B., Marry, V., Dufreche, J.F., Malikova, N., Giffaut, E. & Turq, P., 2007. Modelling water and ion diffusion in clays: A multiscale approach, *C.R. Chim.*, **10**, 1108–1116.

Schoch, R.B., Han, J. & Renaud, P., 2008. Transport phenomena in nanofluidics, Rev.of Modern Phys., **80**, 839–883.

Sondi, I., Biscan, J. & Pravdic, V., 1996. Electrokinetics of pure clay minerals revisited, *J. Colloid Interface Sci.*, **178**, 514–522.

Sonnefeld, J., Lobbus, M. & Vogelsberger, W., 2001. Determination of electric double layer parameters for spherical silica particles under application of the triple layer model using surface charge density data and results of electrokinetic sonic amplitude measurements, *Colloids Surf. A Physicochem. Eng. Asp.*, **195**, 215–225.

Sverjensky, D., 2005. Prediction of surface charge on oxides in salt solutions: Revisions for 1 : 1 (M+L-) electrolytes, *Geochim. Cosmochim. Acta*, **69**, 225–257.

Tournassat, C., Greneche, J.M., Tisserand, D. & Charlet, L., 2004. The titration of clay minerals I. Discontinuous backtitration technique combined with CEC measurements, *J. Colloid Interface Sci.*, **273**, 224–233.

Tournassat, C., Chapron, Y., Leroy, P., Bizi, M. & Boulahya, F., 2009. Comparison of molecular dynamics simulations with triple layer and modified Gouy-Chapman models in a 0.1 M NaCl-montmorillonite system, *J. Colloid Interface Sci.*, **339**, 533–541.

Tournassat, C., Bizi, M., Braibant, G. & Crouzet, C., 2011. Influence of montmorillonite tactoid size on Na-Ca cation exchange reactions, *J. Colloid Interface Sci.*, **364**, 443–454.

Tournassat, C., Grangeon, S., Leroy, P. & Giffaut, E., 2013. Modeling specific pH dependent sorption of divalent metals on montmorillonite surfaces. A review of pitfalls, recent achievements and current challenges, *Am. J. Sci.*, **313**, 395–451.

Tournassat, C., Davis, J.A., Chiaberge, C., Grangeon, S. & Bourg, I.C., 2016. Modeling the Acid–Base Properties of Montmorillonite Edge Surfaces, *Environ. Sci. Technol.*, **50**, 13,436–13,445.

Vinogradov, J., Jaafar, M.Z. & Jackson, M.D., 2010. Measurement of streaming potential coupling coefficient in sandstones saturated with natural and artificial brines at high salinity, *J. Geophys. Res. Solid Earth*, **115**(B12), B12204, doi: 10.1029/2010JB007593.

Vlachy, V., 1999. Ionic effects beyond Poisson-Boltzmann theory, *Annual Review of Physical Chemistry*, **50**, 145–165.

Wang, M., Kang, Q. & Ben-Naim, E., 2010. Modeling of electrokinetic transport in silica nanofluidic channels, *Anal. Chim. Acta*, **664**, 158–164.

Wang, M. & Revil, A., 2010. Electrochemical charge of silica surfaces at high ionic strength in narrow channels, *J. Colloid Interface Sci.*, **343**, 381–386.

Weller, A., Zhang, Z., Slater, L., Kruschwitz, S. & Halisch, M., 2016. Induced polarization and pore radius – A discussion, *Geophysics*, **81**(5), D519–D526.

Wernersson, E., Kjellander, R. & Lyklema, J., 2010. Charge Inversion and Ion−Ion Correlation Effects at the Mercury/Aqueous MgSO4 Interface: Toward the Solution of a Long-Standing Issue, *J. Phys. Chem. C*, **114**, 1849–1866.

Westall, J. & Hohl, H., 1980. A comparison of electrostatic models for the oxide/solution interface, *Adv. Colloid Interface Sci.*, **12**, 265–294.

Xiong, Q., Baychev, T.G. & Jivkov, A.P., 2016. Review of pore network modelling of porous media: Experimental characterisations, network constructions and applications to reactive transport, *J. Contam. Hydrol.*, **192**, 101–117.

Yates, D.E., Levine, S. & Healy, T.W., 1974. Site-binding Model of the Electrical Double Layer at the Oxide/Water interface. *J. Chem. Soc., Faraday Trans.*, **70**, 1807–1818.